Parakhonskiy *et al. J Nanobiotechnol (2015) 13:53*
DOI 10.1186/s12951-015-0111-7

JOURNAL OF NANOBIOTECHNOLOGY

RESEARCH Open Access

The influence of the size and aspect ratio of anisotropic, porous $CaCO_3$ particles on their uptake by cells

Bogdan Parakhonskiy[1,2†], Mikhail V Zyuzin[3†], Alexey Yashchenok[2,4], Susana Carregal-Romero[3], Joanna Rejman[3], Helmuth Möhwald[4], Wolfgang J Parak[3*] and Andre G Skirtach[4,5,6*]

Abstract

Background: Recent reports highlighting the role of particle geometry have suggested that anisotropy can affect the rate and the pathway of particle uptake by cells. Therefore, we investigate the internalization by cells of porous calcium carbonate particles with different shapes and anisotropies.

Results: We report here on a new method of the synthesis of polyelectrolyte coated calcium carbonate particles whose geometry was controlled by varying the mixing speed and time, pH value of the reaction solution, and ratio of the interacting salts used for particle formation. Uptake of spherical, cuboidal, ellipsoidal (with two different sizes) polyelectrolyte coated calcium carbonate particles was studied in cervical carcinoma cells. Quantitative data were obtained from the analysis of confocal laser scanning microscopy images.

Conclusions: Our results indicate that the number of internalized calcium carbonate particles depends on the aspect ratio of the particle, whereby elongated particles (higher aspect ratio) are internalized with a higher frequency than more spherical particles (lower aspect ratio). The total volume of internalized particles scales with the volume of the individual particles, in case equal amount of particles were added per cell.

Keywords: Calcium carbonate, Anisotropic, Uptake, Cells, Internalisation

Background

A multitude of physicochemical properties of particles such as size [1, 2], shape [3–7], charge [8, 9], surface chemistry [10–15], the aggregation state and colloidal stability [16], as well as stiffness [17, 18] directly influences their uptake, intracellular trafficking, and even exocytosis [19] and cytoskeleton re-organization [20]. Different cell types have been used in the experiments including macrophages [21, 22]. Furthermore, these properties are also known to affect particles' in vivo circulation, retention, and bio-distribution [23–26]. Because these diverse parameters are highly entangled [27], experimental determination of the effect of just one parameter remains challenging [28]. For example, the aggregation state plays a particularly important role as it may outweigh the influence of size and charge. On the other hand, the formation of the protein corona simultaneously affects both the aggregation state of particles and their uptake [29]. Therefore, a meaningful analysis necessitates that particles appear in the non-aggregated state in the medium in which they are applied to cells. In case of non-agglomerated particles, the shape of particles can also play a substantial role in their interaction with cells [30, 31]. While the particle shape alone will most likely not determine the pathway by which particles are taken up by cells [32], there are studies indicating that the shape can significantly affect the kinetics of internalization [33]; although in some reports different results have

*Correspondence: Wolfgang.Parak@physik.uni-marburg.de; Andre.Skirtach@UGent.be
†Bogdan Parakhonskiy and Mikhail V Zyuzin contributed equally to this work
[3] Fachbereich Physik, Philipps University of Marburg, Marburg, Germany
[5] NanoBio-Photonics, Ghent University, Ghent, Belgium
Full list of author information is available at the end of the article

been published [34]. The above conclusions apply to both micrometer and nanometer sized particles.

Several studies were conducted to characterize internalization of non-spherical particles and to compare it to spherical particles. For example, polystyrene particles of various sizes and shapes were used to study their internalization by alveolar macrophages [35]. It was found that particles of all shapes were taken up by phagocytosis. However, the internalization velocity [36] depended on the angle between the particle and the initial contact point with the macrophage membrane before internalization. This angle determined whether macrophages initiate uptake or simply spread on the particles [35]. The influence of particle orientation on the interaction between particles and the plasma membrane has been reported by Gilbert et al. [37]. The geometry of the polymer particles was found to influence the rate of endocytosis between disk-shaped particles and spheres of the same volume. Non-spherical particles were reported to have a lower uptake than spherical particles [38] attributed to a larger curvature radius. Furthermore, disk-shaped "flat" particles (i.e. oblate spheroid shape with a low aspect ratio) were reported to have slower internalization velocity in the first hours of incubation with endothelial cells, but the accumulation of particles around the nucleus was similar to that in the long term [33]. This is consistent with the study of Shimoni et al. who reported that the uptake of "flat" polyelectrolyte capsules with decreasing aspect ratio (i.e. ratio of height to width) was lower than the uptake of spherical capsules with the same composition [5]. In that study, the fate of the capsules was also analyzed, and capsules were reported to be localized in lysosomal compartments regardless of their shape. In an additional report, Rubner et al. [39] claim that uptake of flat particles is slowed down to an extent that the particles reside as "backpacks" on the cellular plasma membrane. In a different trend, it was reported that HeLa cells internalize non-spherical hydrogel particles via several different mechanisms, and that they internalize elongated, rod-like particles (i.e. prolate spheroid shape, high aspect ratio) at a higher rate [40]. Although this trend does not hold for lengthy fibers (i.e. for very large aspect ratios); they were found to be internalized at a lower rate than that for round particles [41]. Furthermore, Kolhar et al. [42] reported similar nonspecific uptake for spherical and rod shaped particles in brain and lung endothelial cells using static cell cultures, microfluidics and in vivo studies in mice. These results were further substantiated by a mathematical model. The above mentioned studies were conducted under somewhat different conditions, which may lead to contradictory results. Data from a number of different studies may lead to the general perception that flat particles (i.e. oblate spheroid shape, low aspect ratio) are internalized by cells less efficiently than spherical ones (i.e. aspect ratio = 1), which, in turn, are internalized at a slower rate than particles elongated in one dimension (i.e. prolate spheroid shape, high aspect ratio) as was presented by Chithrani et al. [1]. However, most of these studies suffer from the fact that in addition to the shape of particles typically also the size, aggregation state, and surface chemistry influence their uptake. Furthermore, the results depend on the nature of the particles and type of cells. For example, a recent study made a claim opposite to that outlined above: that flat (i.e. two-dimensionally elongated) as well as rod-like shaped (i.e. one-dimensionally elongated) particles are internalized faster than spherical ones [43]. This only accentuates the need for further studies to create a more comprehensive picture. We note that anisotropy of particles can be achieved by synthesizing them with a higher aspect ratio ("intrinsic anisotropy") or simply by controlling their patchiness ("extrinsic anisotropy") [44–46]. Anisotropic particles adsorb and orient themselves differently even at the border of two different media [47].

In our present work we fabricated anisotropic, polyelectrolyte-coated porous calcium carbonate microparticles ($CaCO_3$) of different shapes and different aspect ratios. These particles were used to investigate the impact of shape on the particle internalization by cervical carcinoma cells. Porous $CaCO_3$ microparticles [48, 49] are attractive because of their acceptable biocompatibility, high surface area to volume ratio, high loading capacity for cargo molecules [50], and low synthesis costs. These particles serve the function of versatile templates for the assembly of hollow polyelectrolyte microcapsules [51–55]. The capsules, fabricated on various templates [56], may be either spontaneously internalized by cells [32, 57–59], or specifically targeted to cells [60]. The porosity of $CaCO_3$, which is often used as a template or core for capsules [48, 56], is one of the key features regarding their application in drug delivery [61], and it has been employed for entrapping dyes, polymers, proteins, polypeptides, inorganic nanoparticles, etc. into the inner volume for sensor applications [62], enzyme-catalyzed reactions [63, 64] or intracellular uptake of capsules [65–68] by cells. In a commonly used preparation method of such particles equal amounts of salt concentrations are mixed producing spherical particles.

In this work we have prepared three different shapes: porous spherical, ellipsoidal, and cuboidal particles [69], using a new method in which unequal concentrations of the interacting salts were used, and compare them with porous spherical calcium carbonate as well as commercially available smooth silica particles serving as control. The particles were coated with polyelectrolytes, so that the surface charges are adjusted, while on the other

hand this coating could allow constructing capsules with the possibility of controlled release [70–74]. During the course of our work, we have also varied the sizes [75] of calcium carbonate particles using yet another innovative approach, in which ethylene glycol was used to slow down the course of the reaction, thus providing data on the influence of the size of particles on their uptake by cells.

Results and discussion

In order to obtain calcium carbonate particles of different shapes, *cf.* Fig. 1, several parameters were adjusted during their synthesis: the stirring time t_s, the presence/absence of ethylene glycol in the aqueous solution in which $CaCl_2$ and Na_2CO_3 were mixed, the sodium carbonate to calcium chloride ratio S, and the pH of the $CaCl_2$ and Na_2CO_3 solutions. By adjusting the stirring time (and to a little extent also the pH of the $CaCl_2$ and Na_2CO_3 solutions), while keeping the concentrations of $CaCl_2$ and Na_2CO_3 equal, we were able to fabricate spherical particles of different sizes (Fig. 2a). The solubility of $CaCO_3$ particles increases by decreasing the pH [76, 77]. At pH = 5 the solubility of $CaCO_3$ particles reaches a critical point, and, if they are stirred at this pH for longer than

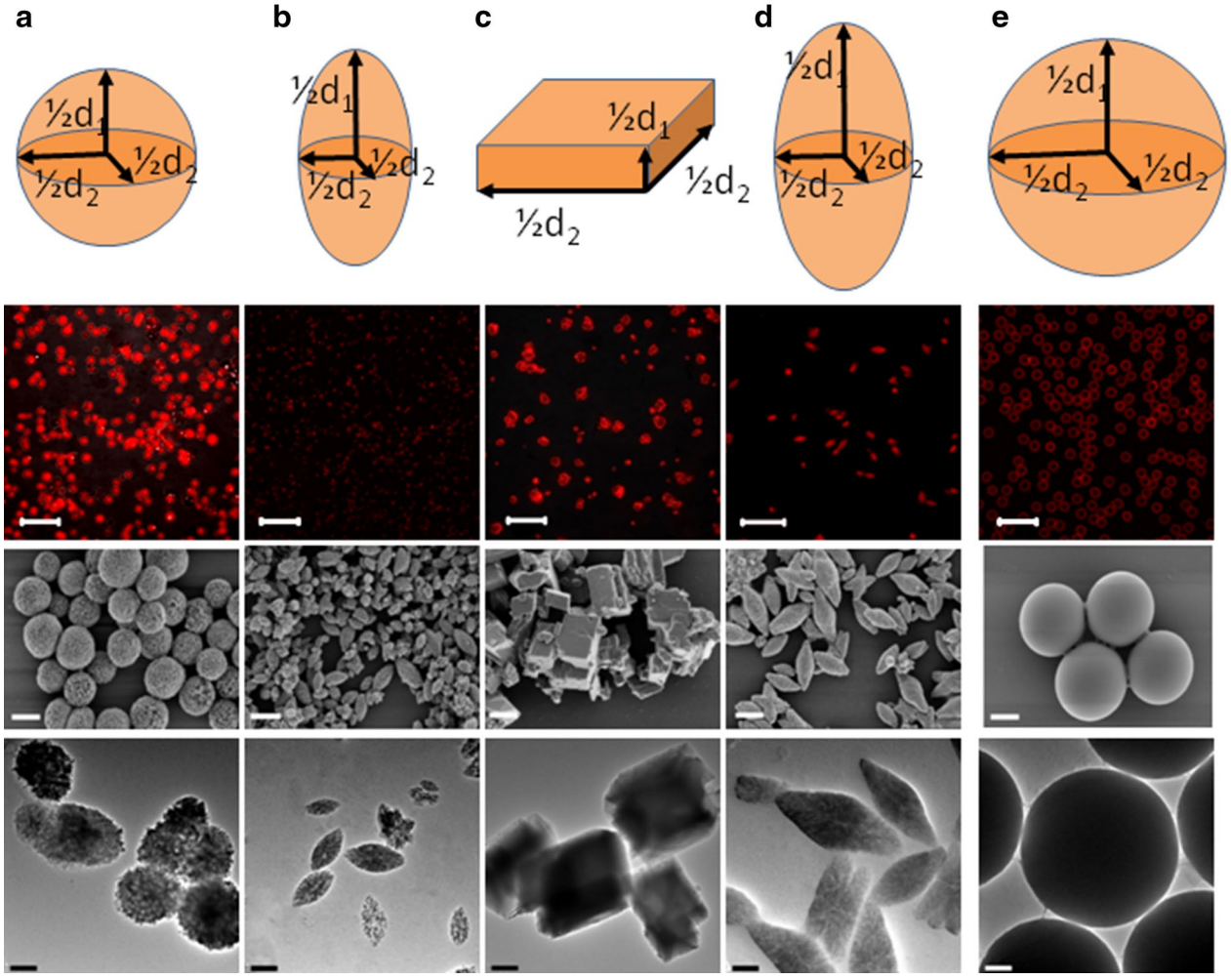

Fig. 1 The *first row* from the *top*: schematics of the geometry of the investigated particles. **a** "Small" spherical $CaCO_3$ particles, **b** "small" ellipsoidal $CaCO_3$ particles, **c** cuboidal $CaCO_3$ particles, **d** "big" ellipsoidal $CaCO_3$ particles, and **e** control "big" spherical SiO_2 particles. All particles have symmetry in the x–y plane. d_1 describes the extension of the particles along the axis of symmetry, and d_2 the extension perpendicular to this axis. The *second row* from the *top*: fluorescence microscopy images of the different particles used in the uptake study as recorded in solution for (**a**) through (**e**). The *scale bars* in all images correspond to 20 μm. The *third row* from the *top*: SEM images of the different particles used in the uptake study for (**a**) through (**e**). The *scale bars* in all images correspond to 2 μm. The *fourth row* from the *top*: TEM images of the different particles used in the uptake study for (**a**) through (**e**). The *scale bars* in all images correspond to 1 μm.

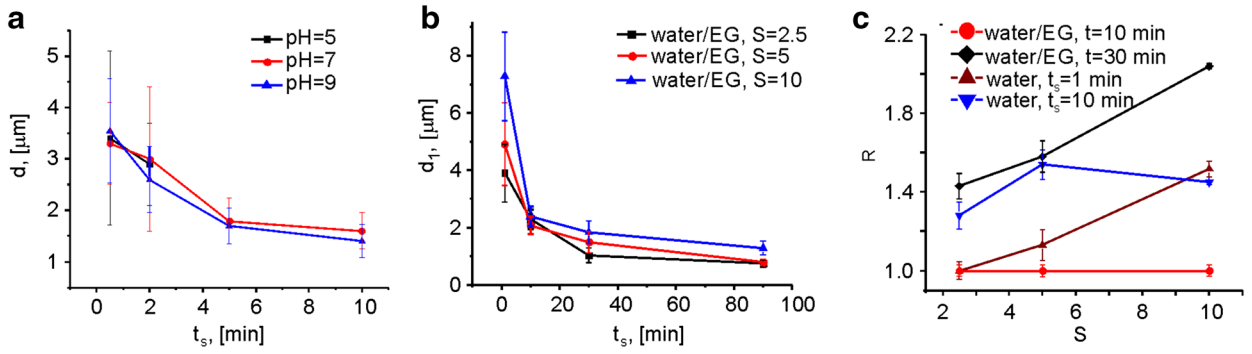

Fig. 2 Tuning the sizes of particles. **a** The size $d = d_1 = d_2$ of spherical $CaCO_3$ particles was tuned by varying the stirring time t of the $CaCl_2$ and Na_2CO_3 solutions at pH values of 5, 7, 9 in pure water solution with a sodium carbonate to calcium chloride ratio S = 1. **b** The size of the long axis d_1 of ellipsoidal $CaCO_3$ particles was tuned by varying the stirring time t_s at certain salt concentration ratios S = 2.5 (*black curve*); 5 (*red curve*); and 10 (*blue curve*) in water/ethylene glycol = 1/5 solutions of pH = 9.5. **c** The aspect ratio R (d_1/d_2) of the $CaCO_3$ particles as a function of S; R was tuned by varying the stirring time t_s in different water and water/EG (ethylene glycol) mixtures at pH = 9.5. The *vertical bars* represent the standard deviation values.

2 min, they completely dissolve. Thus, at low pH the size of $CaCO_3$ particles cannot be modified by controlling the stirring time for longer than 2 min, *cf.* Fig. 2a. Contrary, at higher pH values the size can be better controlled by altering the stirring time. Figure 2a shows the influence of the stirring time obtained with different salt solution pHs (5, 7, 9) when mixing 1 mL of each Na_2CO_3 and $CaCl_2$ (both 0.33 M, i.e. S = 1). The size of the particles decreased when the stirring time was increased, in agreement with the results reported by Sawada et al. [78]. The decrease of particle size was explained by these authors by assuming a phase transition from the unstable vaterite to the stable calcite. This transformation is due to the higher solubility of vaterite compared to calcite. Therefore, the phase transition is energetically favorable [78]. Increasing the pH value from 7 to 9 further decreases the particle size to only a little extent, *cf.* Fig. 2a.

Anisotropic growth could be also achieved by varying the composition of the solvent, e.g. by using mixtures of ethyleneglycol (EG) and water. The presence of EG in the reaction solution decreases the calcium carbonate solubility [75] and changes the time of the reaction between $CaCl_2$ and Na_2CO_3 from minutes to hours. We found that, after the first 30 s of stirring, the lengths of the longest axis of the particles d_1 were around 3 and 6 μm, at salt ratios S = 2.5 and S = 10, respectively (Fig. 2b). Extending the mixing time to 10 min resulted in the formation of particles with $d_1 \approx 2$ μm regardless of salt concentration ratio. The size of the particles slightly decreased to approximately $d_1 \approx 1$ μm upon further stirring. The shape, however, can be also modified in the absence of EG by increasing the salt concentration ratio and the stirring time. Figure 2c shows the change of aspect ratio $R = d_1/d_2$ at different salt concentrations S, two different stirring times t_s, and presence/absence of EG. Overall this approach enables the control of the $CaCO_3$ particle size with d_1 between 0.5 and 6 μm with aspect ratios ranging from 1 to 2. The synthesis of cuboidally shaped particles requires extended time, i.e. stirring, for at least 3 h, in water. Table 1 gives a summary of the obtained $CaCO_3$ particle geometries and of the commercial SiO_2 particles used for the cellular uptake study. We note that although a direct comparison between smooth silica and porous calcium carbonate particles is difficult, the influence of the porosity could be assessed. Inherent monodispersity of silica particles would be an additional factor in this assessment.

The number of internalized particles per cell was evaluated after 24 h incubation by counting the particles inside HeLa cells via fluorescence microscopy and subsequent image analysis. A 24-h-incubation period was chosen because different endocytic processes proceed with different kinetics (e.g. clathrin-mediated endocytosis

Table 1 Particles with different shapes and composed of different materials were used to study their uptake by HeLa cells

Material	Shape	d_1 (μm)	d_2 (μm)	V (μm^3)	R
$CaCO_3$	"Small" spherical	3.3 ± 0.8	3.3 ± 0.8	18.8	1
$CaCO_3$	"Small" ellipsoidal	1.7 ± 0.2	0.9 ± 0.2	0.7	2.0
$CaCO_3$	Cuboidal	2.5 ± 0.9	3.2 ± 1.1	25.6	0.8
$CaCO_3$	"Big" ellipsoidal	3.1 ± 0.5	1.7 ± 0.8	4.7	1.8
SiO_2	"Big" spherical	4.8 ± 0.2	4.8 ± 0.2	58.0	1

The length of the particle extension along the highest symmetry axis d_1 (polar axis), and the width d_2 (equatorial axis) of the particle extension in the plane perpendicular to the highest symmetry axis are given, *cf.* Fig. 1. From d_1 and d_2 the particle volume (V) and aspect ratio (R) were calculated. Data represent the mean value and standard deviation of 30–50 analyzed particles.

proceeds faster than uptake via caveolae). Therefore, a long incubation period ensured that the only parameter influencing the efficiency of uptake was the particle shape and size. The cell cytoskeleton, the nucleus and lysosomes were fluorescently stained and the co-localization of the red fluorescently labeled microparticles within the cellular compartments was evaluated with z-stack images as shown in Fig. 3. Figure 4 shows fluorescence images of HeLa cells that had internalized the differently shaped particles, which are located in the lysosomes, in agreement with previous work [32]. Note that multiple endocytotic pathways are responsible for particle internalization [32]. The histograms shown in Fig. 5a and b represent the number of cells f(N) which internalized the number of N particles and the corresponding cumulative distribution functions (CDFs) p(N) for two sizes of ellipsoidal particles. This figure is an example to show how the CDFs were calculated for all the samples. In particular, smaller ellipsoidal particles were internalized in higher number compared to bigger particles of similar shape. In Fig. 5c the CDFs of "small" spherical, cuboidal, "small" and "big" ellipsoidal and control "big" spherical" particles are shown, which have been obtained similarly to the description of Fig. 5a and b. Cuboidal particles were internalized to the lowest degree. Note that these cuboidal particles had a similar volume as the spherical $CaCO_3$ particles. Thus differences in their internalization indicate the influence of the particle shape (assuming these are individually dispersed particles). Calcium carbonate "small" spherical and "big" ellipsoidal particles, as "big" spherical silica particles were taken up by the cells to similar extent, even though the silica particles have a much larger volume than the $CaCO_3$ particles (58.0 μm^3 for "big" spherical SiO_2 compared with 18.8 and 4.7 μm^3 for "small" spherical and "big" ellipsoidal $CaCO_3$, respectively, *cf.* Table 1). "Small" ellipsoidal particles were internalized to a much higher extent than all other particles, pointing at a correlation between the aspect ratio of particles and their uptake. The higher the aspect ratio the better particles are internalized, which is independent of the microparticle size in first order approximation, *cf.* Fig. 5c.

While confirming the influence of particle shape on cellular uptake, it is necessary to critically discuss the significance of our data. The objective significance is limited by several issues. Firstly, as it can be seen from Fig. 1 there is some variation in shape (and size) of the particles within each batch. Standard particles, such as silica spheres used in this study as control are characterized by a very narrow size distribution. The differently shaped $CaCO_3$ particles as prepared in this study were less mono-disperse. Secondly, it is challenging to vary only one parameter, such as shape, while keeping other parameters, such as size, constant. In the present study the main parameter to be varied was the particle shape, yet as presented in Table 1 it was accompanied by some variations in particle size. Introduction of a scaling parameter, the aspect ratio, helped to demonstrate shape-dependent particle uptake, which in first order was not affected by particle size. Thirdly, the physico-chemical

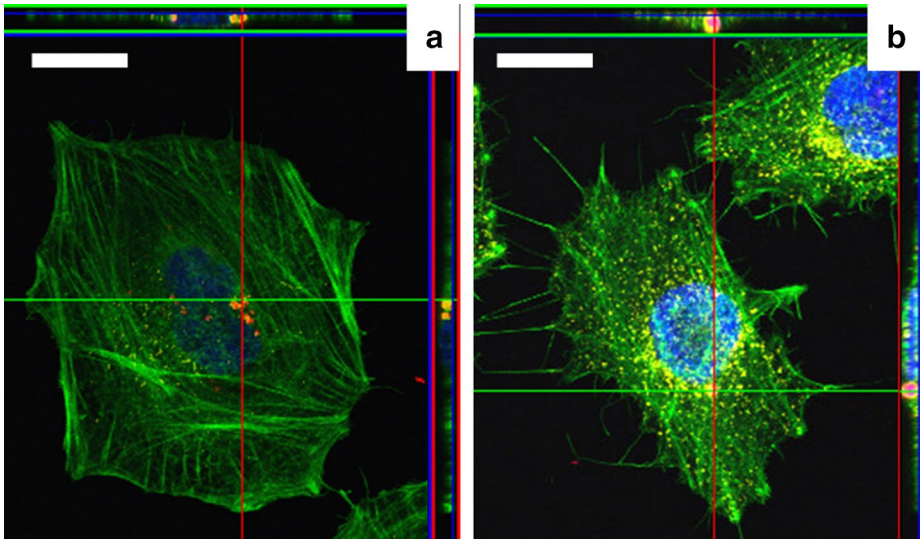

Fig. 3 Orthogonal view from different planes (*x/y*, *x/z* or *y/z*) of the confocal microscope images used to analyze the particle uptake. Examples correspond to: **a** "small" ellipsoidal $CaCO_3$ particles and **b** "big" spherical SiO_2 particles (used as control). Co-localization of fluorescently labeled $CaCO_3$ particles (with TRITC, in *red*) with the lysosomal marker Anti-LAMP1 labeled with DyLight 649 (artificially colored in *yellow*). The HeLa cell´s nucleus was stained with DAPI (in *blue*) and the cytoskeleton with Oregon Green® 488 phalloidin (in *green*). Scale bars correspond to 20 µm.

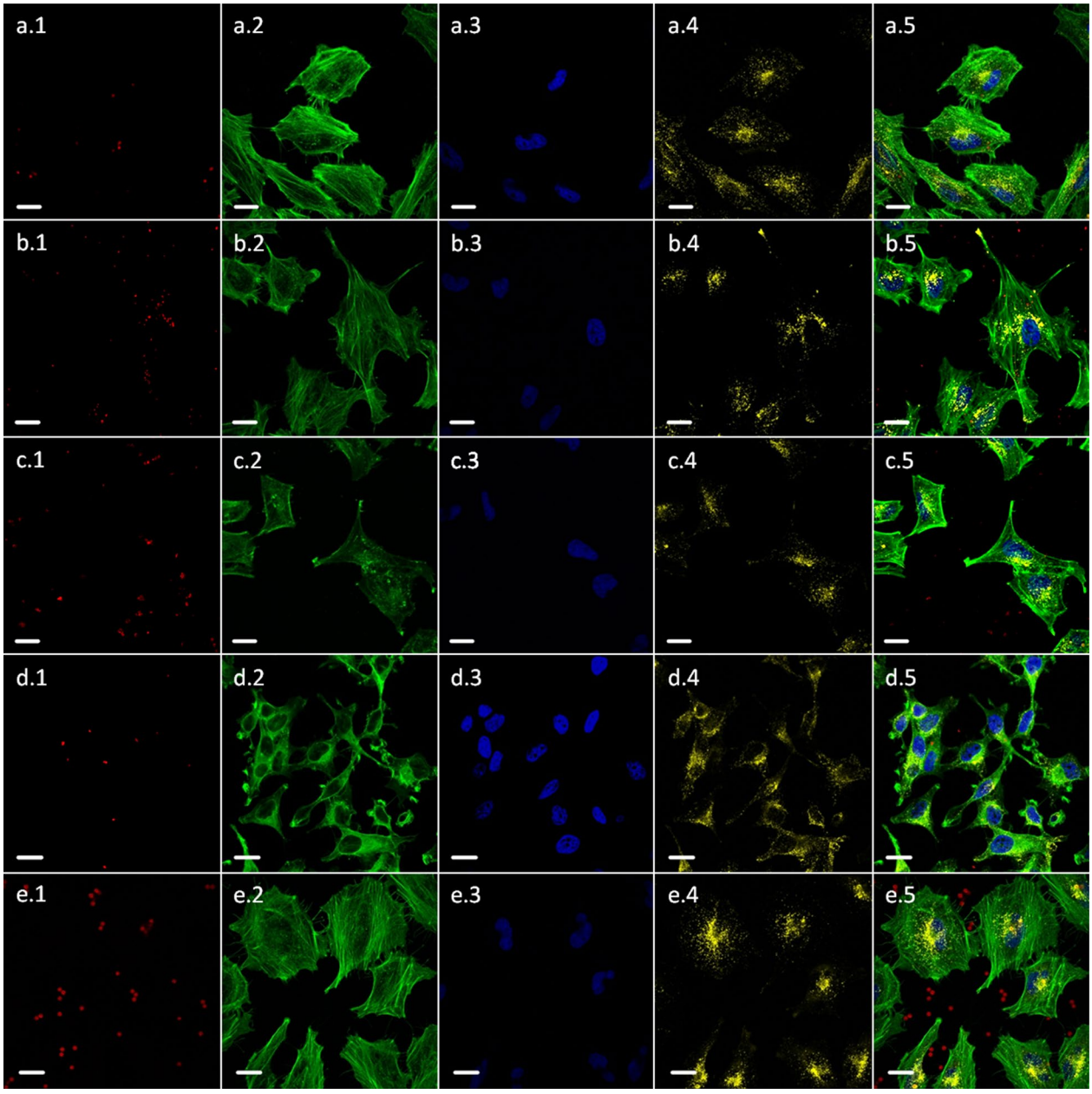

Fig. 4 Confocal images of HeLa cells which internalized differently shaped particles (*red fluorescence*) after incubation for 24 h. **a** "Small" spherical $CaCO_3$ particles, **b** "small" ellipsoidal $CaCO_3$ particles, **c** cuboidal $CaCO_3$ particles, **d** "big" ellipsoidal $CaCO_3$ particles, and **e** "big" spherical SiO_2 particles (used as control). Particles are labeled with TRITC (*red*). Nuclei, lysosomes, and cytoskeletons are fluorescence labeled with DAPI (*blue*), Anti-LAMP1 labeled with DyLight 649 (artificially colored in *yellow*), and Oregon Green® 488 phalloidin (*green*), respectively. *1*, *2*, *3*, *4* and *5* mean the *red*, *green*, *blue* and *yellow* channels and the merged image, respectively. The *scale bars* in all images correspond to 20 μm.

properties of the particles may alter significantly once they are dispersed in cell media (containing proteins and salt). One of the most critical parameters in this context is the stability against agglomeration [8, 13]. Obviously shape- and size-related effects will be altered if particles are no longer individually dispersed, but agglomerated [28]. In this study, particles of the same surface chemistry, i.e. the same outer polyelectrolyte coating, were compared. Thus, while we certainly cannot exclude the presence of agglomerates, still the influence of the cell medium on the aggregation state of different particles should be comparable. Fourthly, in case of limited

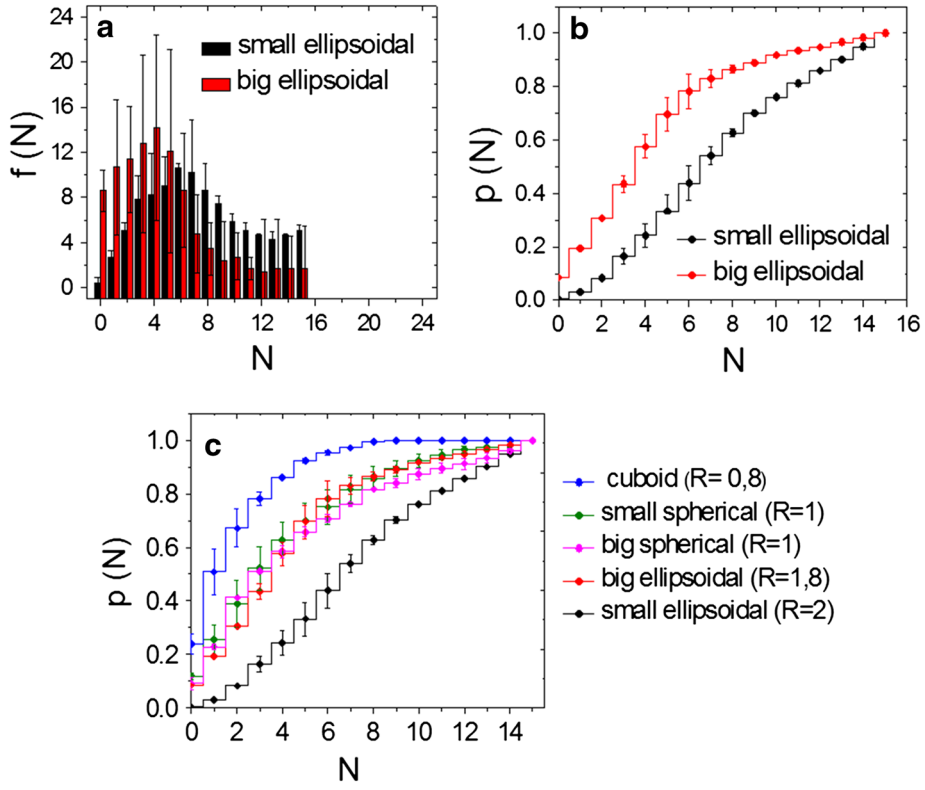

Fig. 5 Influence of size on the uptake of ellipsoidal particles by HeLa cells. **a** Histogram of the frequency f(N) of cells which have internalized N particles per HeLa cell after 24 h of particle incubation with a concentration of 10 added particles per cell. **b** Corresponding cumulative probability plot p(N) showing a higher internalization rate for smaller ellipsoidal $CaCO_3$ particles. The *vertical bars* represent the standard deviation values. **c** Cumulative probability p(N) for N internalized particles per cell for particles with different shape (and size) after 24 h of particle incubation with a cocentration of 10 added particles per cell. Cuboidal $CaCO_3$ (*black dots*), "small" spherical $CaCO_3$ (*green dots*), "big" spherical SiO_2 (*pink dots*), "big" ellipsoidal $CaCO_3$ (*red dots*), and "small" ellipsoidal (*black dots*). All particles had the same surface modification (positively charged layer of PAH). The *vertical bars* represent the standard deviation values.

stability purification is restricted. In Fig. 1 (bottom row) for example, some traces of impurities, besides the actual particles, can be observed. Taken together these limitations indicate that statements have to be interpreted with care. However, our study is in line with several other ones wherein the complex influence of shape is pointed out [37], i.e. wherein the particle uptake is studied analyzing one single parameter—the aspect ratio. Our data confirm that flat particles (R < 1) are incorporated with a lower rate than elongated particles (R > 1). To be more precise, in case the same amount of particles is added to cells, each cell incorporates, on average, a higher number N of elongated in comparison with flat particles.

Quantification of particle uptake by cells in terms of the number of incorporated particles per cell may not always constitute the most appropriate metrics. For example, in the case of drug delivery the relevant measure is the amount of delivered payload or molecular cargo. This can be quantified by presenting the delivered volume per cell V_t. The larger the volume V of a particle, the higher the amount of cargo delivered. The delivered volume per cell can be estimated by calculating the number N of particles internalized per cell multiplied by the volume V (*cf.* Table 1) of each particle ($V_t = N \cdot V$). In this way the CDFs can be converted from number distribution p(N) CDFs into volume distribution $p(V_t)$, *cf.* Additional file 1: Figure S1. The volume distributions demonstrate, that in case cells are exposed to the same amount of particles (with different particle volumes V), the internalized total volume of particles depends on the volume of the individual particles, *cf.* Additional file 1: Figure S1. In other words, in case the same amount of "small" and "big" microparticles is added to cells, the total incorporated volume is higher for the bigger particles, in first order independent of the aspect ratio of the particles. Similar results were obtained when quantifying the delivered surface per cell (Additional file 1: Figures S1, S2). The internalized total surface of particles was higher for larger particles. This indicates that the metrics for quantifying particle uptake by cells is of

utmost importance [26], and results will depend on the selection of the parameters which are investigated. Upon particle uptake (while keeping the number of added particles per cell constant) the number of internalized particles N scales with the aspect ratio of the particles, whereas the total volume of all internalized particles V_t depends on the particle volume V.

We note that development of anisotropic particles [79–84] and capsules [85–88] is seen to influence the transport through the membranes [89], which is significant and can be traced even with the ion level precision [90], and eventual uptake by cells. Such developments are of interest not only for intracellular delivery, but also for artificial and multicompartment capsules [91–93]. In the present work we only investigated one type of cells, one type of surface coating, and one time, and the anisotropy was varied. While the other parameters certainly influence particle–cell interaction as analyzed in previous studies both experimentally [9, 18, 32] and theoretically [36], focus of this work was on analyzing one homologous study, in which only shape (as related to the volume) of the particles was varied.

Conclusions

We have prepared porous calcium carbonate particles with different geometries using a novel method controlling physico-chemical parameters such as pH of solutions, the ratio of salt concentrations, and the duration of the reaction. Subsequently, these particles were used for studying uptake by living cell. The data shown in our study point-out that cellular uptake of particles can be related to simple physico-chemical properties of the particles. One of the most important aspects in cellular uptake studies, often challenging to implement in practice, is to exclusively control the studied parameter. In the presented studies, two parameters are varied: the aspect ratio of the particles and their sizes, i.e. volumes; the influence of these parameters on cell uptake was analyzed.

Our results point out that the internalization rate is increased with increased aspect ratio (excluding very long fibers, wires). If equal amount of particles is added per cell, then the total volume of internalized particles scales with the volume of the individual particles. Smooth, monodisperse silica particles were used an additional control system. The used particle system, porous polyelectrolyte multilayer covered calcium carbonate particles, offers a number of advantages: inexpensiveness, possibility to vary the aspect ratio, porosity, as well as a possibility to control such physicochemical properties as surface charge and surface chemistry. These advantages make the current system an attractive drug delivery platform.

Methods

Materials and methods

For microparticle formation

Poly(allylamine hydrochloride) (PAH, M_w = 70 kDa), poly(sodium 4-styrenesulfonate) sodium salt (PSS, M_w = 70 kDa), tetramethylrhodamine isothiocynate-dextran (TRITC-dextran, M_w = 70 kDa), calcium chloride dihydrate ($CaCl_2 \cdot 2H_2O$), and sodium carbonate (Na_2CO_3) were purchased from Sigma-Aldrich, Germany. Ethylene glycol solution (99%) was purchased from Alfa Aesar. In all procedures Milli-Q water was used with resistivity >18 MΩ.

For cell culture

Trypsin–EDTA was purchased from GIBCO. Dulbecco's Essential Minimum Eagle's Medium (EMEM), Penicillin–Streptomycin (P/S) was delivered by Sigma-Aldrich. Phosphate Buffered Saline (PBS) and fetal serum bovine were purchased from Biochrom.

For immunostaining

The primary monoclonal mouse anti-human LAMP1 antibody was obtained from the Developmental Studies Hybridoma Bank. The secondary antibody donkey anti-mouse IgG (H + L) conjugated with DyLight 649 and bovine serum albumin (BSA) *IgG-free* were delivered by Jackson Immuno Research Laboratories. (4′,6-diamidino-2-phenylindol, dilactate) (DAPI) and Oregon Green® 488 phalloidin were purchased from Life Technologies. Saponin from quillaja bark (≥10%) was delivered by Sigma-Aldrich. Fluoromount-G was obtained from SouthernBiotech. Glycine (≥99%) was purchased from Roth. A confocal scanning microscope LSM 510 Meta (Zeiss), equipped with a diode laser (405 nm; 30 mW), an Ar-laser (458, 477, 488,514 nm; 30 mW), a HeNe-laser (543 nm; 1 mW), and a HeNe-laser (633 nm; 5 mW) from Carl Zeiss was used for the uptake studies. The staining protocols used for the uptake studies are explained in detail in the Additional file 1 and have been reported previously by Kast et al. [30].

Synthesis of calcium carbonate particles

Calcium carbonate microparticles of various shapes, Fig. 1, were fabricated using a combination of unequal salt concentration and addition of ethylene glycol [69] while controlling the reaction mixing time and pH of the solutions. Briefly, for spherical $CaCO_3$ microparticles 1 mL of Na_2CO_3 (0.33 M, pH 8) was injected into a glass vessel and then an equal volume of $CaCl_2$ (0.33 M, pH 12) was injected and stirred at 600 rpm for 1 min. This time the pH was not adjusted. Further, the diameter of spherical particles was tuned from 3.5 to 1.5 μm by changing the pH of the salt solutions ($CaCl_2$

and Na_2CO_3), by addition of HCl/NaOH, and the stirring time as it is described in Fig. 2a. Small ellipsoidal $CaCO_3$ particles (1.7 ± 0.1 μm) were produced in a mixture of water and ethylene glycol. 1 mL of Na_2CO_3 (1 M, pH = 9.5) was injected into a glass vessel containing 10 mL ethylene glycol (EG) under stirring. Then 1 mL of $CaCl_2$ (0.1 M, pH = 9.5) was mixed with 10 mL of EG; it was subsequently thoroughly stirred and was added to the glass vessel containing 1 mL of Na_2CO_3 and 10 mL of EG. The mixture was further stirred at 600 rpm for 30 min. The pH of the salt solutions was adjusted to 9.5 by addition of HCl/NaOH. The sodium carbonate to calcium chloride concentration ratio, S, was in this case equal to 10. The obtained particles had 1.7 ± 0.1 μm length for the longest axis (d_1), 0.9 ± 0.2 μm for the shortest axis (d_2) and an aspect ratio $R = d_1/d_2 = 2$. The size of ellipsoidal particles could be also tuned by changing the stirring time and by slightly modifying the salt concentration ratio, *cf.* Fig. 1. Large ellipsoidal $CaCO_3$ particles were synthesized in water (without EG) at conditions identical to that of small ellipsoidal particles. Cuboidally shaped particles were prepared by mixing 1 mL $CaCl_2$ (1 M, pH 8) and 1 mL Na_2CO_3 (1 M, pH 12) in a glass flask under stirring (without EG). The mixture was further stirred at 600 rpm for at least 3 h. All particle solutions were thoroughly washed immediately after the synthesis with water and alcohol in order to remove un-reacted components and residual ethylene glycol. Then the particles were placed for 1 h in a conventional oven set at 70°C. All differently shaped $CaCO_3$ particles were subsequently labeled with fluorescent dextran (TRITC) by entrapping these molecules inside the porous $CaCO_3$. To that end the $CaCO_3$ microparticles were incubated in 0.5 mL of aqueous TRITC-dextran solution (1 mg/mL) for 30 min. Then particles were washed twice with water. In the final step two layers of the synthetic polyelectrolytes poly(allylamine hydrochloride) (PAH, 2 mg/mL in 0.5 M NaCl, positively charged) and poly(sodium 4-styrenesulfonate) (PSS, 2 mg/mL in 0.5 M NaCl, negatively charged) were adsorbed onto the surface of the $CaCO_3$ particles via the layer-by-layer (LbL) technique [51–54]. Since the surface charge of cuboidal particles is almost neutral and in order to facilitate polyelectrolyte adsorption they were coated first with PSS to produce the following sequence of layers: (PSS/PAH/PSS). It should be pointed out that the $CaCO_3$ cores were not dissolved at the end of the assembly procedure. Commercial, originally negatively charged silica particles (4.8 ± 0.2 μm, Microparticles GmbH, Germany) were coated with one layer of PAH, then incubated with TRITC-dextran and subsequently terminated with PSS. This time the fluorescent molecules labeled the shell of silica particles. Both $CaCO_3$ and silica particles are terminated with a PSS shell and thus were negatively charged at neutral pH.

Characterization of particles

The size of the particles was determined by optical microscopy, Fig. 1. The shape of dried particles was confirmed by taking scanning electron microscopy (SEM) and transmission electron microscopy (TEM) images, Fig. 1, the third and fourth row, respectively. The volumes (V) of differently shaped particles were calculated using the following formulas. For spherical particles $V = \frac{4}{3}\pi\left(\frac{d}{2}\right)^3$, where $d = d_1 = d_2$ is the particle diameter. For cuboidal particles $V = d_1 \cdot d_2^2$, assuming "flat" particles as square base with side lengths d_1 and a height of d_2. For ellipsoidal particles $V = \frac{4}{3}\pi\frac{d_1}{2}\cdot\left(\frac{d_2}{2}\right)^2$ with the diameters d_1 of the long axis and d_2 of the short axis of an ellipsoid with prolate spheroid shape, respectively. All particles show symmetry around one axis. The extension of the particles along this axis is the particle height d_1. The extensions of the particles perpendicular to this axis are the particle widths d_2, *cf.* Fig. 1. The aspect ratio R was calculated as $R = d_1/d_2$, e.g. for "flat" particles $R < 1$, for spherical particles $R = 1$, and for elongated particles $R > 1$.

After the polyelectrolyte layer deposition (last PSS layer) the particles had neutral or negative zeta potential. For larger spherical particles the value was measured to be ~−41.4 ± 0.9 mV, while for small spheres, small ellipse and cubes the values were −23.4 ± 0.5, −28.2 ± 0.2 and −25.8 ± 0.6, respectively. Zeta-potentials for "big" elliptic particles were measured to be close to the neutral value.

Cell experiments

For uptake studies cervical carcinoma HeLa cells 35,000 cells were seeded for 24 h on sterilized round cover slips (Carl Roth) placed on the bottom of 12-well plates with 18 mm diameter (TTP). Each well was filled with 700 μL of Eagle's Minimum Essential Medium (EMEM), which contained 10% vol of fetal bovine serum (FBS), 1% vol of the antibiotics penicillin and streptomycin (P/S) at 37°C and 5% CO_2 atmosphere. After the first 24 h, cells were incubated with differently shaped particles with a ratio of 10 particles/cell for another 24 h. The concentration of particles was calculated with a hemocytometer, which was possible due to the large size of the particles that allowed for visualization with optical microscopy. After that, cover slips were transferred to a flat surface covered with parafilm (Carl Roth) to proceed with the fixation of the cells and the staining of the cell compartments following several steps. Firstly, cells were fixed with 100 μL of a 4% paraformaldehyde solution for 30 min. Then, cells were permeabilized with 70 μL of a solution of 0.5 mg/

mL saponin and 5 mg/mL glycine in phosphate buffered saline (PBS) for 5 min. After that, cells were blocked with additional 70 µL of 20 mg/mL solution of bovine serum albumin (BSA) for 30 min. After blocking the cells were incubated for 1 h with primary antibodies LAMP-1 (70 µL, 1 mg/mL) and washed three times with blocking solution. Then, cells were incubated for 1 h with (70 µL, 4 mg/mL) fluorophore-conjugated (DyLight 649) secondary antibodies, 4′-6-diamidino-2-phenylindole (DAPI), and phalloidin-tetramethylrhodamine. The secondary antibodies labeled with DyLight 649 were used to stain lysosomal compartments. DAPI was used to stain the nucleus and phalloidin to stain the cytoskeleton. In a last step, cells were washed three times with PBS and finally Fluoromount-G was used to fix the cover slips above cells on glass slides (76 × 26 mm) [24]. Fluorescence micrographs of HeLa cells with the internalized particles were recorded with a confocal microscope (Zeiss LSM 510 Meta Confocal Microscope) equipped with a laser diode emitting at 405 nm (used to visualize the nuclei labeled with DAPI, emission filter: LP 420), an argon laser with a line at 488 nm (used to visualize the cytoskeleton labeled with Oregon Green® 488 phalloidin, emission filter BP 505–550) and a helium–neon laser for excitation at 543 nm (used to visualize the microparticles labeled with TRITC, emission filter: BP 560–615) and at 633 nm (used to visualize the lysosomes labeled with DyLight 649, emission filter LP 420), respectively. To reduce the scanning time we used the same channel and emission filter to visualize DAPI and DyLight 649. Lysosomes stained with DyLight 649 were artificially stained in yellow. Images were taken with a Plan-Apochromat 63×/1.40 Oil DIC M27 objective, and the pin hole was set to 0.86–1.32 airy units. All images were recorded and analyzed as z-stacks. The number of internalized particles per cell was then determined. In average, 600–700 particles were counted and at least 100 different cells were analyzed for every experiment that was repeated twice. Dividing and not fully depicted cells were not considered for analysis. Taking into account the staining of: (1) the actin network which delineated the cell shape (green fluorescence coming from fluorescently-labeled phalloidin), (2) the lysosomal compartments (artificial yellow color coming from DyLight 649-conjugated secondary antibody), and (3) the nucleus inside each cell (blue fluorescence coming from DAPI), microparticles (in red fluorescently-labeled) surrounded by DyLight 649 and phalloidin were classified as intracellular. Microparticles adherent to the outer cell plasma membrane and in between the grown cells were clearly distinguished from the microparticles with intracellular location, *cf.* Figs. 3 and 4 [32]. Based on these confocal images, histograms showing the number of internalized particles per cell f(N), as well as the corresponding cumulative distribution functions (CDFs) p(N) were generated, *cf.* Fig. 5 and Additional file 1: Figure S1. Standard deviations were calculated from the deviation of the independent f(N) or CDFs of two different experiments per each data set. The histogram f(N) describes the frequency f, i.e. the number of events, in which cells with exactly N internalized particles were observed. The CDF p(N) indicates the probability, that a cell contains N or less particles internalized. For example, $p(N = 3)$ is the probability to find cells with either 0, 1, 2, or 3 internalized particles. CDFs are directly calculated from histograms where $p(N) = \sum_{i=0}^{N} f(i) / \sum_{i=0}^{\infty} f(i)$ and they are used to make the differences of particle uptake easier to be visualized. The CDFs are normalized and thus $0 \leq p(N) \leq 1$ [30]. All data can be found in the Additional file 1.

Additional file

Additional file 1: Figure S1. Cumulative probability p(N) for the total internalized particle volume V_t per cell ($p(V_t)$). Particles had different shape (and size): "small" ellipsoidal $CaCO_3$ (black dots), "big" ellipsoidal $CaCO_3$ (red dots), cuboidal $CaCO_3$ (blue dots), "small" spherical $CaCO_3$ (green dots) and "big" spherical SiO_2 (pink dots). The plot is based on the data shown in Figure 9. The vertical bars represent the standard deviation values. **Figure S2.** Parameters of particles and cumulative probability. (a) Volume (V), surface (S) and surface-to-volume ratio (S/V) of the five different kinds of particles. (b) Cumulative probability plot $p(S_t)$ for total surface S_t of internalized particles per cell for particles with different shape (and size) after 24 h of particle incubation with a concentration of 10 particles added per cell. The total internal surface corresponds to the surface S of the particles times the number N of internalized particles per cell. Data are displayed for cuboidal $CaCO_3$ (blue dots), "small" spherical $CaCO_3$ (green dots), "big" spherical SiO_2 (pink dots), "big" ellipsoidal $CaCO_3$ (red dots), and "small" $CaCO_3$ ellipsoidal particles (black dots). All particles had the same surface modification (positively charged layer of PAH). The vertical bars represent the standard deviation values. **Table SI-1.** Raw data of the histogram shown in Figure 5a for "small" and "big" ellipsoidal particles. f(N) is the frequency of cells which have internalized N particles per HeLa cell after 24 h of particle incubation with a concentration of 10 added particles per cell. SD stands for standard deviation. **Table SI-2.** Raw data of the cumulative probability plot shown in Figure 5b for "small" and "big" ellipsoidal particles. p(N) is the cumulative probability of cells, which have internalized N particles per HeLa cell after 24 h of particle incubation with a concentration of 10 added particles per cell. SD stands for standard deviation. **Table SI-3.** Raw data of the cumulative probability plot shown in Figure 5c for all types of particles. p(N) is the cumulative probability of cells, which have internalized N particles per HeLa cell after 24 h of particle incubation with a concentration of 10 added particles per cell. SD stands for standard deviation, sph. stands for spherical, ellip. stands for ellipsoidal and cub. stands for cuboidal. **Table SI-4.** Raw data of the cumulative total internalized particle volume V_t per cell ($p(V_t)$) shown in Figure S1. SD stands for standard deviation, sph. stands for spherical, ellip. stands for ellipsoidal and cub. stands for cuboidal.

Abbreviations

$CaCO_3$: calcium carbonate; DAPI: diamidino-2-phenylindole; PSS: poly(sodium 4-styrenesulfonate) sodium salt; PAH: Poly(allylamine hydrochloride); BSA: bovine serum albumin; EG: ethyleneglycol.

Authors' contributions

BP, AY synthesized particles and arranged for electron microscopy and confocal microscopy images of the particles and contributed to writing of the manuscript; MVZ, SCR and JR conducted cell culture measurements,

analyzed the data, arranged for confocal microscopy, electron microscopy and contributed to writing of the manuscript. HM, WJP and AGS designed the experiments and contributed to writing of the manuscript. All authors read and approved the final manuscript.

Author details
[1] Shubnikov Institute of Crystallography, Russian Academy of Science, Moscow, Russia. [2] Institute of Nanostructures and Biosystems, Saratov State University, Saratov, Russia. [3] Fachbereich Physik, Philipps University of Marburg, Marburg, Germany. [4] Department of Interfaces, Max-Planck Institute of Colloids and Interfaces, Potsdam, Germany. [5] NanoBio-Photonics, Ghent University, Ghent, Belgium. [6] Department of Molecular Biotechnology, Ghent University, Ghent, Belgium.

Acknowledgements
We thank Rona Pitschke for electron microscopy images. BP thanks the Marie-Curie foundation for a fellowship. AY acknowledges the Alexander von Humboldt-Stiftung for a scholarship. The authors are grateful to Xiang Yu for the TEM images. This work was partly funded by LOEWE (project Synchembio to WJP) and the European Commission (project FutureNanoNeeds to WJP). We would like also to thank EU FP-7-People-IRSES project 'DINaMIT', and the Government of the Russian Federation (grant number 14.Z50.31.0004 to support scientific research projects implemented under the supervision of leading scientists at Russian institutions and Russian institutions of higher education), and RFBR research project No 15-29-01172. AGS acknowledges support of FWO (Fonds Wetenschappelijk Onderzoek) Vlaanderen and BOF (Bijzonder Onderzoekfonds, University of Ghent, Belgium). B.P. is a postdoctoral fellow of the Research Foundation-Flanders (FWO, FWO-Vlaanderen).

Compliance with ethical guidelines

Competing interests
The authors declare that they have no competing interests.

Received: 16 April 2015 Accepted: 28 July 2015
Published online: 04 September 2015

References

1. Chithrani BD, Ghazani AA, Chan WCW (2006) Determining the size and shape dependence of gold nanoparticle uptake into mammalian cells. Nano Lett 6:662–668
2. Lerch S, Dass M, Musyanovych A, Landfester K, Mailaender V (2013) Polymeric nanoparticles of different sizes overcome the cell membrane barrier. Eur J Pharm Biopharm 84:265–274
3. Bhaskar S, Pollock KM, Yoshida M, Lahann J (2010) Towards designer microparticles: simultaneous control of anisotropy, shape, and size. Small 6:404–411
4. Daum N, Tscheka C, Neumeyer A, Schneider M (2012) Novel approaches for drug delivery systems in nanomedicine: effects of particle design and shape. Wiley Interdiscip Rev Nanomed Nanobiotechnol 4:52–65
5. Shimoni O, Yan Y, Wang YJ, Caruso F (2013) Shape-dependent cellular processing of polyelectrolyte capsules. ACS Nano 7:522–530
6. Meng H, Yang S, Li ZX, Xia T, Chen J, Ji ZX et al (2011) Aspect ratio determines the quantity of mesoporous silica nanoparticle uptake by a small GTPase-dependent macropinocytosis mechanism. ACS Nano 5:4434–4447
7. Holt B, Lam R, Meldrum FC, Stoyanov SD, Paunov VN (2007) Anisotropic nano-papier mache microcapsules. Soft Matter 3:188–190
8. Huhn D, Kantner K, Geidel C, Brandholt S, De Cock I, Soenen SJH et al (2013) Polymer-coated nanoparticles interacting with proteins and cells: focusing on the sign of the net charge. ACS Nano 7:3253–3263
9. Javier AM, Kreft O, Alberola AP, Kirchner C, Zebli B, Susha AS et al (2006) Combined atomic force microscopy and optical microscopy measurements as a method to investigate particle uptake by cells. Small 2:394–400
10. Wattendorf U, Kreft O, Textor M, Sukhorukov GB, Merkle HP (2008) Stable stealth function for hollow polyelectrolyte microcapsules through a poly(ethylene glycol) grafted polyelectrolyte adlayer. Biomacromolecules 9:100–108
11. Jiang XE, Dausend J, Hafner M, Musyanovych A, Rocker C, Landfester K, Mailander V et al (2010) Specific effects of surface amines on polystyrene nanoparticles in their interactions with mesenchymal stem cells. Biomacromolecules 11:748–753
12. He CB, Hu YP, Yin LC, Tang C, Yin CH (2010) Effects of particle size and surface charge on cellular uptake and biodistribution of polymeric nanoparticles. Biomaterials 31:3657–3666
13. Delehanty JB, Blanco-Canosa JB, Bradburne CE, Susumu K, Stewart MH, Prasuhn DE et al (2013) Site-specific cellular delivery of quantum dots with chemoselectively-assembled modular peptides. Chem Commun 49:7878–7880
14. Parakhonskiy BV, Foss C, Carletti E, Fedel M, Haase A, Motta A et al (2013) Tailored intracellular delivery via a crystal phase transition in 400 nm vaterite particles. Biomater Sci 1:1273–1281
15. Tang R, Moyano DF, Subramani C, Yan B, Jeoung E, Tonga GY et al (2014) Rapid coating of surfaces with functionalized nanoparticles for regulation of cell behavior. Adv Mater 26:3310–3314
16. Caballero-Diaz E, Pfeiffer C, Kastl L, Rivera-Gil P, Simonet B, Valcarcel M et al (2013) the toxicity of silver nanoparticles depends on their uptake by cells and thus on their surface chemistry. Part Part Syst Charact 30:1079–1085
17. Bedard MF, Munoz-Javier A, Mueller R, del Pino P, Fery A, Parak WJ et al (2009) On the mechanical stability of polymeric microcontainers functionalized with nanoparticles. Soft Matter 5:148–155
18. Hartmann R, Weidenbach M, Neubauer M, Fery A, Parak WJ (2015) Stiffness-dependent in vitro uptake and lysosomal acidification of colloidal particles. Angew Chem Int Ed 54:1365–1368
19. Kim CS, Le NDB, Xing YQ, Yan B, Tonga GY, Kim C et al (2014) The role of surface functionality in nanoparticle exocytosis. Adv Healthc Mater 3:1200–1202
20. Wang B, Zhang YY, Mao ZW, Gao CY (2012) Cellular uptake of covalent poly(allylamine hydrochloride) microcapsules and its influences on cell functions. Macromol Biosci 12:1534–1545
21. Doshi N, Mitragotri S (2010) Macrophages recognize size and shape of their targets. PLoS One 5:e10051
22. Leclerc L, Boudard D, Pourchez J, Forest V, Marmuse L, Louis C et al (2012) Quantitative cellular uptake of double fluorescent core-shelled model submicronic particles. J Nanopart Res 14:1221
23. Simone EA, Dziubla TD, Muzykantov VR (2008) Polymeric carriers: role of geometry in drug delivery. Expert Opin Drug Deliv 5:1283–1300
24. De Jong WH, Hagens WI, Krystek P, Burger MC, Sips A, Geertsma RE (2008) Particle size-dependent organ distribution of gold nanoparticles after intravenous administration. Biomaterials 29:1912–1919
25. Sonavane G, Tomoda K, Makino K (2008) Biodistribution of colloidal gold nanoparticles after intravenous administration: effect of particle size. Colloids Surf B Biointerfaces 66:274–280
26. Lankveld DPK, Oomen AG, Krystek P, Neigh A, Troost-de Jong A, Noorlander CW et al (2010) The kinetics of the tissue distribution of silver nanoparticles of different sizes. Biomaterials 31:8350–8361
27. Velev OD, Gupta S (2009) Materials fabricated by micro- and nanoparticle assembly—the challenging path from science to engineering. Adv Mater 21:1897–1905
28. Rivera-Gil P, De Aberasturi DJ, Wulf V, Pelaz B, Del Pino P, Zhao YY et al (2013) The challenge to relate the physicochemical properties of colloidal nanoparticles to their cytotoxicity. Acc Chem Res 46:743–749
29. Yan Y, Gause KT, Kamphuis MMJ, Ang CS, O'Brien-Simpson NM, Lenzo JC et al (2013) Differential roles of the protein corona in the cellular uptake of nanoporous polymer particles by monocyte and macrophage cell lines. ACS Nano 7:10960–10970
30. Hutter E, Boridy S, Labrecque S, Lalancette-Hebert M, Kriz J, Winnik FM et al (2010) microglial response to gold nanoparticles. ACS Nano 4:2595–2606
31. Liu SB, Wei L, Hao L, Fang N, Chang MW, Xu R et al (2009) Sharper and faster "nano darts" kill more bacteria: a study of antibacterial activity of individually dispersed pristine single-walled carbon nanotube. ACS Nano 3:3891–3902
32. Kastl L, Sasse D, Wulf V, Hartmann R, Mircheski J, Ranke C et al (2013) Multiple internalization pathways of polyelectrolyte multilayer capsules into mammalian cells. ACS Nano 7:6605–6618
33. Yoo JW, Doshi N, Mitragotri S (2010) Endocytosis and intracellular distribution of PLGA particles in endothelial cells: effect of particle geometry. Macromol Rapid Commun 31:142–148

34. Herd H, Daum N, Jones AT, Huwer H, Ghandehari H, Lehr CM (2013) Nanoparticle geometry and surface orientation influence mode of cellular uptake. ACS Nano 7:1961–1973
35. Champion JA, Mitragotri S (2006) Role of target geometry in phagocytosis. Proc Natl Acad Sci USA 103:4930–4934
36. Decuzzi P, Ferrari M (2008) The receptor-mediated endocytosis of nonspherical particles. Biophys J 94:3790–3797
37. Gilbert JB, O'Brien JS, Suresh HS, Cohen RE, Rubner MF (2013) Orientation-specific attachment of polymeric microtubes on cell surfaces. Adv Mater 25:5948–5952
38. Florez L, Herrmann C, Cramer JM, Hauser CP, Koynov K, Landfester K et al (2012) How shape influences uptake: interactions of anisotropic polymer nanoparticles and human mesenchymal stem cells. Small 8:2222–2230
39. Swiston AJ, Gilbert JB, Irvine DJ, Cohen RE, Rubner MF (2010) Freely suspended cellular "backpacks" lead to cell aggregate self-assembly. Biomacromolecules 11:1826–1832
40. Gratton SEA, Ropp PA, Pohlhaus PD, Luft JC, Madden VJ, Napier ME et al (2008) The effect of particle design on cellular internalization pathways. Proc Natl Acad Sci USA 105:11613–11618
41. Geng Y, Dalhaimer P, Cai SS, Tsai R, Tewari M, Minko T et al (2007) Shape effects of filaments versus spherical particles in flow and drug delivery. Nat Nanotechnol 2:249–255
42. Kolhar P, Anselmo AC, Gupta V, Pant K, Prabhakarpandian B, Ruoslahti E et al (2013) Using shape effects to target antibody-coated nanoparticles to lung and brain endothelium. Proc Natl Acad Sci USA 110:10753–10758
43. Agarwal R, Singh V, Jurney P, Shi L, Sreenivasan SV, Roy K (2013) Mammalian cells preferentially internalize hydrogel nanodiscs over nanorods and use shape-specific uptake mechanisms. Proc Natl Acad Sci USA 110:17247–17252
44. Glotzer SC, Solomon MJ (2007) Anisotropy of building blocks and their assembly into complex structures. Nat Mater 6:557–562
45. Pawar AB, Kretzschmar I (2010) Fabrication, assembly, and application of patchy particles. Macromol Rapid Commun 31:150–168
46. Kohler D, Madaboosi N, Delcea M, Schmidt S, De Geest BG, Volodkin DV et al (2012) Patchiness of embedded particles and film stiffness control through concentration of gold nanoparticles. Adv Mater 24:1095–1100
47. Sharp EL, Al-Shehri H, Horozov TS, Stoyanov SD, Paunov VN (2014) Adsorption of shape-anisotropic and porous particles at the air-water and the decane-water interface studied by the gel trapping technique. Rsc Adv 4:2205–2213
48. Volodkin D (2014) CaCO3 templated micro-beads and -capsules for bioapplications. Adv Colloid Interface Sci 207:306–324
49. Trushina DB, Bukreeva TV, Kovalchuk MV, Antipina MN (2014) CaCO3 vaterite microparticles for biomedical and personal care applications. Mater Sci Eng, C 45:644–658
50. Parakhonskiy BV, Yashchenok AM, Donatan S, Volodkin DV, Tessarolo F, Antolini R et al (2014) Macromolecule loading into spherical, elliptical, star-like and cubic calcium carbonate carriers. ChemPhysChem 15:2817–2822
51. Ariga K, Lvov YM, Kawakami K, Ji QM, Hill JP (2011) Layer-by-layer self-assembled shells for drug delivery. Adv Drug Deliv Rev 63:762–771
52. Becker AL, Johnston APR, Caruso F (2010) Layer-by-layer-assembled capsules and films for therapeutic delivery. Small 6:1836–1852
53. Rivera Gil P, del Mercato LL, del-Pino P, Munoz-Javier A, Parak WJ (2008) Nanoparticle-modified polyelectrolyte capsules. Nano Today 3:12–21
54. Skirtach AG, Yashchenok AM, Mohwald H (2011) Encapsulation, release and applications of LbL polyelectrolyte multilayer capsules. Chem Commun 47:12736–12746
55. Vergaro V, Scarlino F, Bellomo C, Rinaldi R, Vergara D, Maffia M et al (2011) Drug-loaded polyelectrolyte microcapsules for sustained targeting of cancer cells. Adv Drug Deliv Rev 63:847–863
56. Parakhonskiy BV, Yashchenok AM, Konrad M, Skirtach AG (2014) Colloidal micro- and nano-particles as templates for polyelectrolyte multilayer capsules. Adv Colloid Interface Sci 207:253–264
57. Sukhorukov GB, Rogach AL, Zebli B, Liedl T, Skirtach AG, Kohler K et al (2005) Nanoengineered polymer capsules: tools for detection, controlled delivery, and site-specific manipulation. Small 1:194–200
58. De Koker S, De Geest BG, Cuvelier C, Ferdinande L, Deckers W, Hennink WE et al (2007) In vivo cellular uptake, degradation, and biocompatibility of polyelectrolyte microcapsules. Adv Funct Mater 17:3754–3763
59. Javier AM, Kreft O, Semmling M, Kempter S, Skirtach AG, Bruns OT et al (2008) Uptake of colloidal polyelectrolyte-coated particles and polyelectrolyte multilayer capsules by living cells. Adv Mater 20:4281–4287
60. Cortez C, Tomaskovic-Crook E, Johnston APR, Radt B, Cody SH, Scott AM et al (2006) Targeting and uptake of multilayered particles to colorectal cancer cells. Adv Mater 18:1998
61. del Mercato LL, Ferraro MM, Baldassarre F, Mancarella S, Greco V, Rinaldi R et al (2014) Biological applications of LbL multilayer capsules: from drug delivery to sensing. Adv Colloid Interface Sci 207:139–154
62. Yashchenok AM, Borisova D, Parakhonskiy BV, Masic A, Pinchasik BE, Mohwald H et al (2012) Nanoplasmonic smooth silica versus porous calcium carbonate bead biosensors for detection of biomarkers. Ann Phys 524:723–732
63. Yashchenok AM, Delcea M, Videnova K, Jares-Erijman EA, Jovin TM, Konrad M et al (2010) Enzyme reaction in the pores of CaCO3 particles upon ultrasound disruption of attached substrate-filled liposomes. Angew Chem Int Ed 49:8116–8120
64. Islan GA, Cacicedo ML, Bosio VE, Castro GR (2015) Development and characterization of new enzymatic modified hybrid calcium carbonate microparticles to obtain nano-architectured surfaces for enhanced drug loading. J Colloid Interface Sci 439:76–87
65. del Mercato LL, Abbasi AZ, Ochs M, Parak WJ (2011) Multiplexed sensing of ions with barcoded polyelectrolyte capsules. ACS Nano 5:9668–9674
66. Sukhorukov GB, Volodkin DV, Gunther AM, Petrov AI, Shenoy DB, Mohwald H (2004) Porous calcium carbonate microparticles as templates for encapsulation of bioactive compounds. J Mater Chem 14:2073–2081
67. Rivera-Gil P, De Koker S, De Geest BG, Parak WJ (2009) Intracellular processing of proteins mediated by biodegradable polyelectrolyte capsules. Nano Lett 9:4398–4402
68. Sami H, Maparu AK, Kumar A, Sivakumar S (2012) Generic delivery of payload of nanoparticles intracellularly via hybrid polymer capsules for bioimaging applications. PLoS One 7:e36195
69. Yashchenok A, Parakhonskiy B, Donatan S, Kohler D, Skirtach A, Mohwald H (2013) Polyelectrolyte multilayer microcapsules templated on spherical, elliptical and square calcium carbonate particles. J Mater Chem B 1:1223–1228
70. Sato K, Seno M, Anzai JI (2014) Release of insulin from calcium carbonate microspheres with and without layer-by-layer thin coatings. Polymers 6:2157–2165
71. Palankar R, Pinchasik BE, Schmidt S, De Geest BG, Fery A, Mohwald H et al (2013) Mechanical strength and intracellular uptake of CaCO3-templated LbL capsules composed of biodegradable polyelectrolytes: the influence of the number of layers. J Mater Chem B 1:1175–1181
72. Reibetanz U, Schonberg M, Rathmann S, Strehlow V, Gose M, Lessig J (2012) Inhibition of human neutrophil elastase by alpha(1)-antitrypsin functionalized colloidal microcarriers. ACS Nano 6:6325–6336
73. Wuytens P, Parakhonskiy B, Yashchenok A, Winterhalter M, Skirtach A (2014) Pharmacological aspects of release from microcapsules—from polymeric multilayers to lipid membranes. Curr Opin Pharmacol 18:129–140
74. Ye CH, Combs ZA, Calabrese R, Dai HQ, Kaplan DL, Tsukruk VV (2014) Robust microcapsules with controlled permeability from silk fibroin reinforced with graphene oxide. Small 10:5087–5097
75. Parakhonskiy BV, Haase A, Antolini R (2012) Sub-micrometer vaterite containers: synthesis, substance loading, and release. Angew Chem Int Ed 51:1195–1197
76. Tai CY, Chen FB (1998) Polymorphism of CaCO3 precipitated in a constant-composition environment. AIChE J 44:1790–1798
77. Svenskaya Y, Parakhonskiy B, Haase A, Atkin V, Lukyanets E, Gorin D et al (2013) Anticancer drug delivery system based on calcium carbonate particles loaded with a photosensitizer. Biophys Chem 182:11–15
78. Sawada K (1997) The mechanisms of crystallization and transformation of calcium carbonates. Pure Appl Chem 69:921–928
79. Kozlovskaya V, Chen J, Tedjo C, Liang X, Campos-Gomez J, Oh JW et al (2014) pH-responsive hydrogel cubes for release of doxorubicin in cancer cells. J Mater Chem B 2:2494–2507
80. Lattuada M, Hatton TA (2011) Synthesis, properties and applications of Janus nanoparticles. Nano Today 6:286–308
81. Sacanna S, Pine DJ (2011) Shape-anisotropic colloids: building blocks for complex assemblies. Curr Opin Colloid Interface Sci 16:96–105
82. Walther A, Muller AHE (2013) Janus particles: synthesis, self-assembly, physical properties, and applications. Chem Rev 113:5194–5261
83. Lee KJ, Yoon J, Lahann J (2011) Recent advances with anisotropic particles. Curr Opin Colloid Interface Sci 16:195–202

84. Shields CW, Zhu S, Yang Y, Bharti B, Liu J, Yellen BB et al (2013) Field-directed assembly of patchy anisotropic microparticles with defined shape. Soft Matter 9:9219–9229
85. Shchepelina O, Kozlovskaya V, Kharlampieva E, Mao WB, Alexeev A, Tsukruk VV (2010) Anisotropic micro- and nano-capsules. Macromol Rapid Commun 31:2041–2046
86. Shchepelina O, Kozlovskaya V, Singamaneni S, Kharlampieva E, Tsukruk VV (2010) Replication of anisotropic dispersed particulates and complex continuous templates. J Mater Chem 20:6587–6603
87. Delcea M, Madaboosi N, Yashchenok AM, Subedi P, Volodkin DV, De Geest BG et al (2011) Anisotropic multicompartment micro- and nano-capsules produced via embedding into biocompatible PLL/HA films. Chem Commun 47:2098–2100
88. Lisunova M, Dorokhin A, Holland N, Shevchenko VV, Tsukruk VV (2013) Assembly of the anisotropic microcapsules in aqueous dispersions. Soft Matter 9:3651–3660
89. Alexeev A, Uspal WE, Balazs AC (2008) Harnessing Janus nanoparticles to create controllable pores in membranes. ACS Nano 2:1117–1122
90. Palankar R, Pinchasik BE, Khlebtsov BN, Kolesnikova TA, Mohwald H, Winterhalter M et al (2014) Nanoplasmonically-induced defects in lipid membrane monitored by ion current: transient nanopores versus membrane rupture. Nano Lett 14:4273–4279
91. Hosta-Rigau L, Shimoni O, Stadler B, Caruso F (2013) Advanced subcompartmentalized microreactors: polymer hydrogel carriers encapsulating polymer capsules and liposomes. Small 9:3573–3583
92. Delcea M, Yashchenok A, Videnova K, Kreft O, Mohwald H, Skirtach AG (2010) Multicompartmental micro- and nanocapsules: hierarchy and applications in biosciences. Macromol Biosci 10:465–474
93. Musyanovych A, Landfester K (2014) Polymer micro- and nanocapsules as biological carriers with multifunctional properties. Macromol Biosci 14:458–477